Evaporation phenomena in the atomization of superheated liquids and their impact on the spray characteristics

A. Günther[1*], K.-E. Wirth
Institute of Particle Technology, Friedrich-Alexander-University Erlangen-Nuremberg, Germany
a.guenther@lfg.uni-erlangen.de and k.e.wirth@lfg.uni-erlangen.de

Abstract

The atomization of superheated liquids enables a spray disintegration by the means of thermal energy. No additional gas phase is applied, a vapor phase is generated by evaporation out of the fluid media itself. Accordingly evaporation phenomena have great impact on the resulting spray quality. By the means of transparent glass nozzles bubbles generated inside the capillary are analyzed. Characteristics of the spray are then linked to the evaporation phenomena. In addition the results of steel nozzles are compared to the more academic results of the glass nozzle. The investigations are done by mass flux measurements and optical means including PIV (Particle Image Velocimetry) and Shadowgraphy.

Introduction

There are various modifications of spraying processes including pressure atomization and two-substance spraying all implemented in order to enhance the surface of fluid media. The application of two-substance nozzles allows the generation of comparably fine particle distributions even with fluids of high viscosity yielding moderate to high throughput. Some of the finest particle size distributions are produced by two-component nozzles with inner mixing, among them nozzles for effervescent atomization [1]. The gas phase is bubbled into the fluid flow, leading to an enhancement of spray disintegration [2]. Although this method requires only a small amount of gas in comparison to other two-substance nozzles, there is still an additional material component present that could hamper following processing steps. Furthermore a comparably complex geometry has to be applied for this process. The named drawbacks can be circumvented by the atomization of superheated liquids. In this special modification of a multiphase spraying process thermal energy is utilized in addition to low pressure energy in order to generate a biphasic flow inside the nozzle capillary. The spraying fluid is heated beyond its boiling point but hindered to evaporate by applying a process pressure higher than the vapour pressure corresponding to the given temperature. With a counter-pressure of 1 bar a pressure difference exists over the nozzle. Evaporation or flashing begins when the pressure falls beneath the vapour pressure yielding a biphasic flow. When the generated bubbles get into contact with the surrounding they burst since they exhibit an inner pressure corresponding to the vapour pressure of the applied fluid temperature. By this a radial velocity component is induced and the disintegration of the fluid jet is enhanced [3, 4, 5].

Applying the atomization of superheated liquids the geometry of the nozzles can be rather simple (for example full cone nozzles) to yield particle sizes comparable to those produced by two-substance nozzles. Accessorily no additional gas has to be inserted since vapour is generated out of the fluid itself. Depending on process parameter like pressure or temperature the disintegration of the fluid and hence the droplet size distribution can be adjusted in the range of mm to µm. Since a hot fluid flow exits the nozzle evaporation is taking place yielding a mass flow away from droplets reducing coalescence processes [9]. In addition evaporation effects allow an energy reduction in spray drying applications.

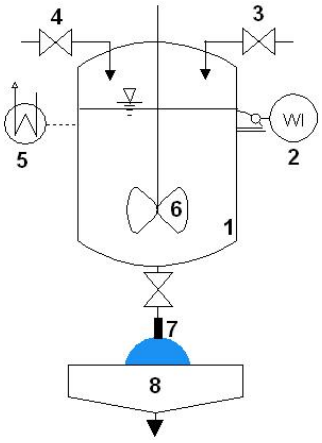

Figure 1 Spraying plant

Influencing variables besides process parameters and fluid properties are the L/D-ratio of the nozzle [5, 6, 7] and the roughness of the nozzle inner capillary [8] which have an influence on the resulting flow through the nozzle and accordingly on the spray characteristics. Modifications of those geometries alter the evaporation inside the nozzle capillary and hence the distribution of the vapour bubbles [10]. The focus of this paper therefore is the analysis of the flow through the nozzle and its impact on the spray quality by mass flux analysis and optical measurement techniques including Particle Image Velocimetry (PIV) and Shadowgraphy.

* Corresponding author: a.guenther@lfg.uni-erlangen.de

Experimental Methods

The plant used for the following experiments is depicted in Figure 1. The main part is a pressure vessel (1) with a volume of ca. 20 l. The vessel is mounted via a load cell (HBM, 200 kg max, accuracy 0.02 %) (2) on a movable framework allowing a continuous measurement of the total weight yielding the mass flux during a spraying event. In the upper part of the vessel the process fluid, deionized water, can be inserted (3). The maximum overpressure p_0 can be adjusted to 6 bar by pressurized air (4). Heating jackets surround the vessel (5), enabling the system to be warmed up to the maximum of 150°C. In order to achieve a homogenous temperature distribution inside the pressure vessel a stirrer (6) keeps the fluid in continuous motion during the preheating period. In the downstream part of the vessel the nozzle (7) is located. Beneath the spray a suction system (8) removes vapor that would hamper the optical measurements.

For the atomization capillary nozzle with a simple geometry are deployed. Glass nozzles offer the possibility to monitor the bubble distribution inside the nozzle capillary while steel nozzles represent the actual shape and material applied in a technical process. Both nozzle shapes are depicted in Figure 2. The two have the same L/D-ratio (L/D = 20) and the same diameter of the nozzle capillary (D = 0.9 mm). Differences are given by the inlet into the nozzle capillary where the glass nozzles has a rather smooth one and the steel nozzle`s is quite sharp. In addition the surface roughness is higher in the case of the steel nozzle because of the fabrication methods which is drawing for the glass nozzle and drilling in the case of the steel nozzle. The last difference is given by the outlet geometry of both nozzles. The glass nozzle shows a flat outlet while the steel nozzle has a pointed one.

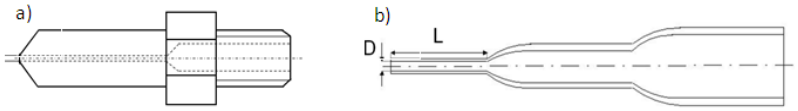

Figure 2 Applied nozzles
a) Steel nozzle b) Glass nozzle

Particle Image Velocimetry (PIV) is used for velocity measurements and Shadowgraphy for analyzing spray morphology and evaporation inside the nozzle capillary. For both measurement techniques a CCD – Camera (2048 x 2048 Pixel) from PCO is applied. In the case of PIV it is located in a 90° angle in respect to a laser light sheet that passes through the center of the spray. The analysis is executed in a measurement field of 90 mm x 40 mm. For Shadowgraphy measurements a green LED is located opposite to the CCD – Camera with the process spray in between. The measurement area for Shadowgraphy pictures of the nozzle capillary is 40 mm x 35 mm.

Results and Discussion

In order to analyze the amount of vapor generated in the nozzle shadowgraphic pictures of the glass nozzle capillary are taken. Two examples are shown in Figure 3. The process conditions are the same for both pictures. As one can see the amount and also the distribution of the vapor is greatly varying. In order to characterize the distribution of vapor 100 pictures taken at a frame rate of 7 Hz are analyzed regarding the number and cross section area distribution of the contained bubbles. The sizes of the bubbles where analyzed using the Software “Envision Patternation”. The morphology of the bubbles also greatly varies as can be seen in Figure 3. In order to facilitate the analysis of the bubbles the extent of each bubble was determined in radial and vertical orientation. The cross sectional area of the bubbles is approximated by equating all bubbles by rectangles. In Figure 4 the results for the analysis of the bubble dimensions in vertical (y – direction) and radial orientation (x –direction) are delineated. In addition the absolute numbers of bubbles per pictures for the given temperatures are listed in Figure 3. The bubble size in radial direction is limited by the dimension of the nozzle capillary diameter which is 0.9 mm. Therefore all bubbles filling the whole diameter cross section have a radial dimension of 0.9 mm. That is why there is a peak at this size for all of the applied nozzles. Regarding the smaller sizes one can observe some differences. For 130°C the measured bubbles are rather small. The radial size distribution is shifted to bigger characteristic lengths for a higher superheat at 140°C. At 150°C the measured sizes are smaller than at 130°C and 140°C. For the vertical

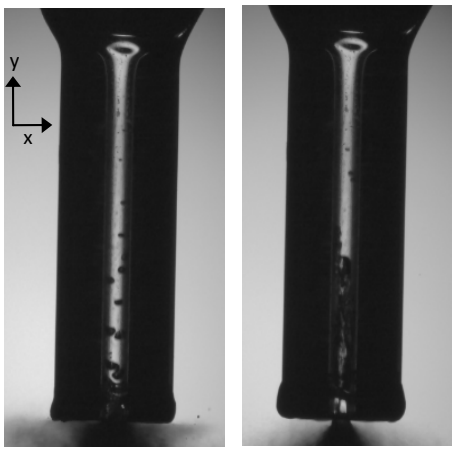

Figure 3 Shadowgraphic pictures of the nozzle capillary
T_0 = 150°C, p_0 = 5 bar

distribution a similar trend is observed. A process temperature of 150°C yields a peak for the smallest sizes which is more pronounced for 130°C and especially for 140°C where the biggest bubbles can be found. Regarding the absolute number of bubbles monitored in each picture one can see that it is enhanced with temperature with a major jump from 140°C to 150°C. That is in accordance with literature [10] that states that the higher the superheat the higher the tendency of the system to evaporate.

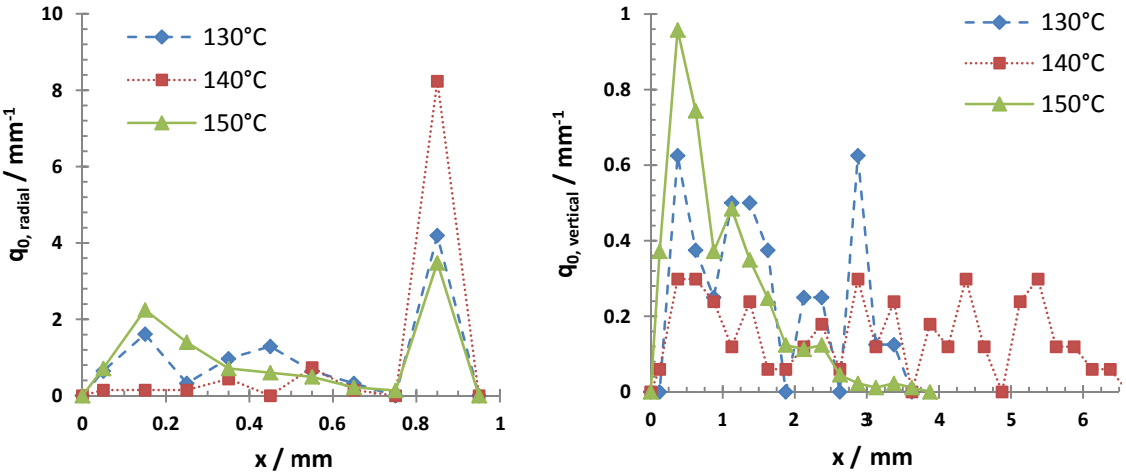

Figure 4 Number density distribution of bubbles inside nozzle capillary as a function of the characteristic lengths for p_0 = 5 bar in

a) Radial (x-) direction b) Vertical (y-) direction

Table 1 Absolute number of bubbles per picture; p_0 = 5 bar

T / °C	N per picture / -
130	0.32
140	0.68
150	3.66

Considering Table 1 and Figure 4 one can categorize the bubble distributions at small (130°C), medium (140°C) and high (150°C) superheat as follows (Table 2):

Table 2 Bubble categories in respect to the process temperature

T / °C	Bubble size	Number of bubbles
130	Mostly Small	Low
140	Mostly Big	Low
150	Most Small	High

Park et al. [10] monitored the bubble distributions in the process of the superheated atomization. They concluded that low superheat yields bubbly flow – a lot of small bubbles dispersed over the whole nozzle cross-section. For medium superheat slug flow is observed which means that bigger bubbles are measured that leave the nozzle in a pulsing mode. At high superheat they observe annular flow, here the fluid is only located at the nozzle capillary sides, the core of is filled with vapor. The temperatures they applied were in the range of 100°C – 120°C so a lot smaller than those applied for the depicted experiments. Nevertheless the experiments still yielded higher bubble densities in comparison to the results shown in this paper. Reasons for this behavior can probably be allocated to the geometry differences between the applied nozzles. Their glass nozzles are partially made of steel and also featured a rather sharp inlet. That means there were more surface roughnesses given hence more boiling seeds for evaporation. On the other hand the flow was likely to be detached from the nozzle wall yielding an enhanced turbulence. Both effects lead to increased evaporation. But despite all differences the trend that more bubbles are formed with increased superheat still holds true.

r content for erheating

T /°C	α / %
130	1.97
140	9.59
150	4.12

In order to analyze the amount of generated vapor, the cross section area density distribution (bubbles equated by rectangles) is depicted in Figure 5. By assuming the depth of the approximated bubble rectangles identical with the diame-

ter of the capillary, the vapor content in the capillary for the different operating conditions can be calculated (see equation 1). The results are depicted in Table 3.

$$\alpha = \frac{\text{Average crosssection area of vapor per picture}(T_i)}{\text{Average crossection of nozzle capillary}} \quad (1)$$

The density distribution shows that the vapor cross sectional area has a peak for rather small for 130°C and 150°C. The peak for 130°C is more pronounced but a broader peak is given for the highest applied superheat. For 140°C the cross sectional area distribution is remarkably enhanced in comparison.

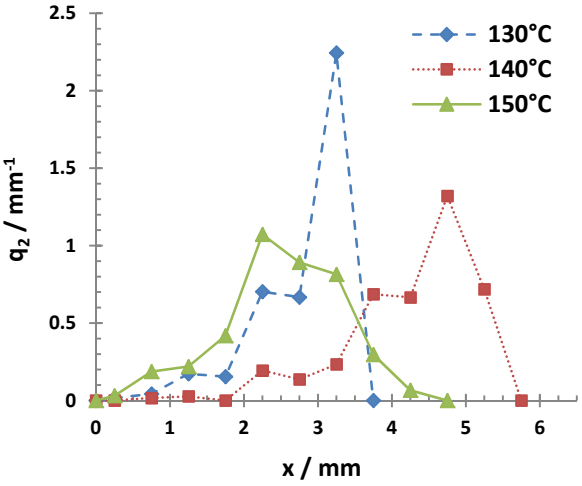

Figure 5 Cross sectional area distribution for vapor bubbles at various superheating; p_0 = 5 bar

Theoretically one would have expected the amount of vapor to rise according to the enhancement of the process temperature since the driving force for evaporation, the vapor pressure p_V, increases simultaneously. An explanation for the reduction of vapor for high superheat is given regarding the Jacob Number which is defined according equation (2):

$$Ja = \frac{\rho_f \cdot c_{p,f} \cdot (T_i - T_{sat})}{\rho_v \cdot \Delta h_v} \quad (2)$$

According to Neroorkar [11] the Jacob Number is the ratio of the amount of energy stored inside the system versus the energy needed to evaporate. Consequently the higher the Jacob Number the higher will the amount of generated vapor be. The course of the dimensionless quantity versus temperature is depicted in Figure 6.
At low temperatures up to a point of 140°C the Jacob Number is rising hence there is more energy for evaporation available. For higher temperatures the Jacob number is reduced. There the disposable energy is still enhanced but the amount of required energy increases more in comparison since the density of the resulting vapor phase is higher. In consequence less vapor can be generated at temperatures higher than 140°C.

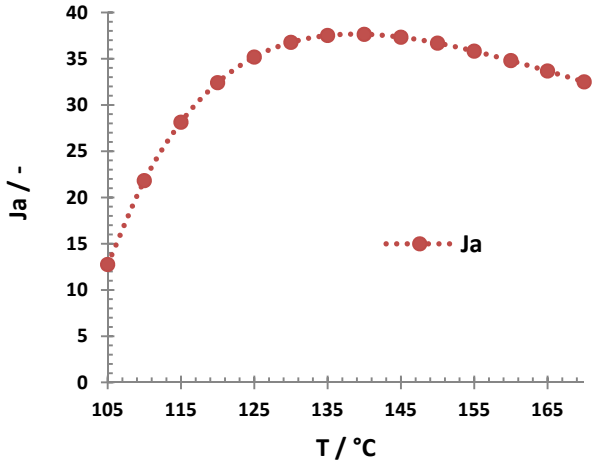

Figure 6 Jacob Number versus temperature

Up to this point only the changes for the vapor phase inside the nozzle capillary have been shown. The influences of those alterations on the spray are pictured in Figure 7. In order to compare those changes to a nozzle with more than an academic application the spray morphology for a steel nozzle with a similar geometry is presented at the same process parameters. At a given temperature of 25°C a pure fluid jets is exited into the surrounding. Superheat (hence a temperature higher than 100°C) is needed to initiate jet disintegration. The spray contour is widening with enhanced temperature for both nozzle types. The disintegration seems to be more violent for the steel nozzle. This can be attributed to the fact that there are more and also

more distinct boiling seeds in the form of surface roughness in the case of a steel capillary. The evaporation inside the system is enhanced by those and the spray break-up is improved accordingly.

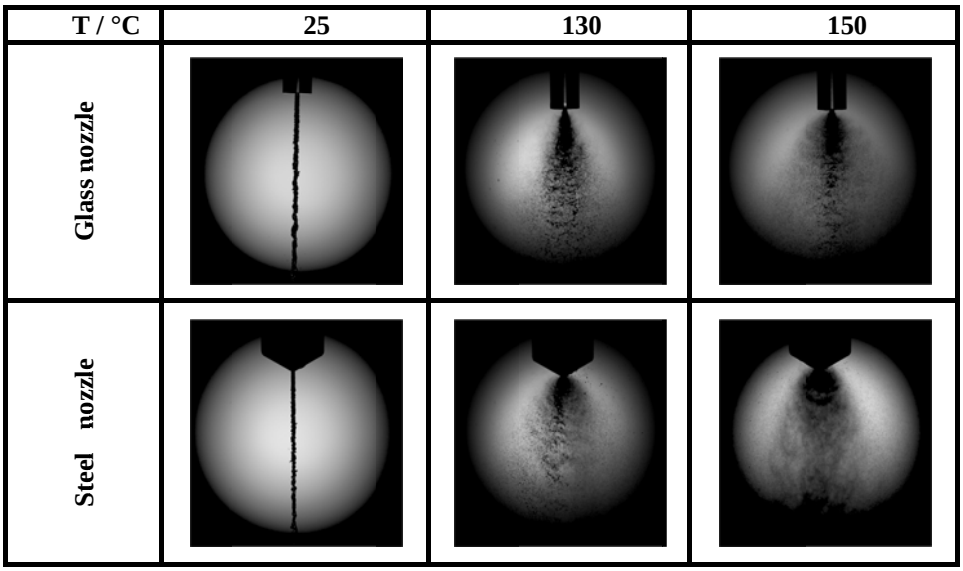

Figure 7 Morphology changes for glass and steel nozzle for different temperatures

The changes in evaporation can also be observed analyzing the measured mass flux. Since the mass flux is measured via weight loss of the complete system the problems known for throughput measurements do not occur. This is depicted in Figure 8 by applying the dimensionless mass flux F versus the cavitation number p* which are defined according to equation (3)

$$F = \frac{M_{T_i}}{M_{25°C}} \propto \sqrt{\frac{p_0 - p_v(T_i)}{p_0 - p_\infty}} \tag{3}$$

The cavitation number is the ratio of two pressure differences and is reduced with rising vapor pressure p_v or decreasing surrounding pressure p_∞. The lower the dimensionless quantity the more vapor is theoretically generated. The dimensionless mass flux F is defined as the ratio of the mass flux at a given process temperature T_i versus subcooled, completely fluid mass flux at 25°C. The limiting cases are given by F = 1 (dashed line = pure fluid flow) and the dotted square root dependency according to equation (3) for ideal evaporation.

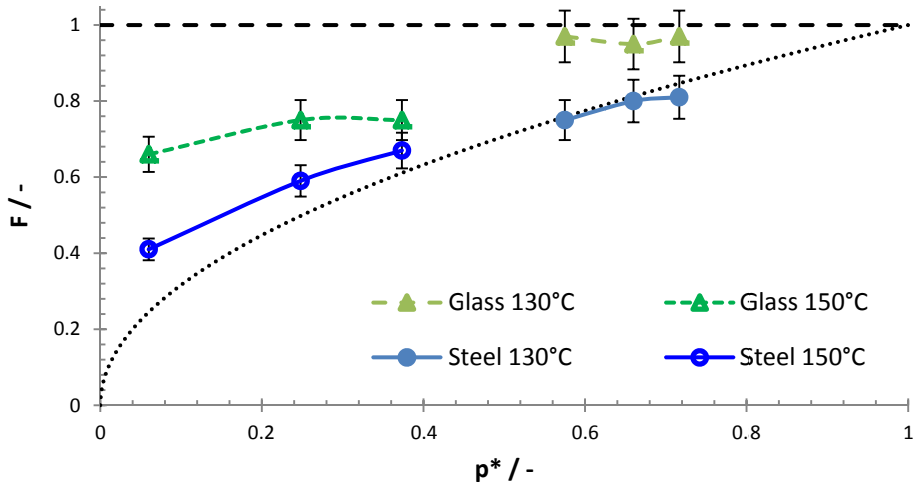

Figure 8 Mass flux changes for different nozzles; p_0 = 4 bar - 6 bar

For a low superheat at 130°C the steel nozzle shows nearly ideal evaporation while the glass nozzle offers measurement points that are nearer to a fluid behavior. For a high superheat (150°C) both nozzles offer an enhanced evaporation. The steel nozzle again shows an increased tendency for vapor generation. The deviations

from the ideal curve for the steel nozzle at high superheating can be explained by the same arguments as the reduction of vapor content with temperature by cooling effects and the influence of heat conduction.

The resulting droplet velocity distributions are measured for both nozzles by PIV. The results can be seen in Figure 9.

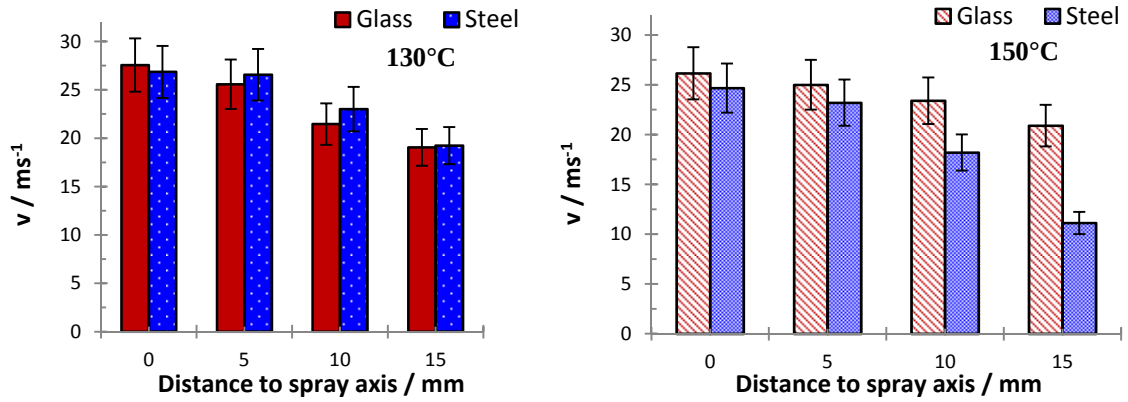

Figure 9 Droplet velocity distribution; p_0 = 5 bar

The measurements are done in a distance of 60 mm from the nozzle outlet. It was not possible to conduct measurements nearer to the nozzle because of the high droplet density. The results for both process temperatures (130°C, 150°C) show that the velocity is reduced towards the edge of the spray for the glass nozzle as well as for the steel nozzle. The spray density is lowered toward the spray margin therefore the interactions between spray and surrounding are enhanced resulting in smaller droplet velocities. Furthermore the velocities measured on the spray axis, the location of smallest interaction between fluid phase and surrounding gas phase, are quite similar for all nozzles and temperatures. Comparing the course of velocity for both temperatures it can be observed that at a lower superheat higher droplet velocities are achieved which are also quite similar for glass and steel nozzle. At 130°C evaporation is far from ideal according to Figure 8 therefore a rather undistributed spray is generated. Bigger droplets are less decelerated by the surrounding hence higher velocities result for lower superheat. More pronounced differences regarding the velocity are observed for 150°C. Droplets generated by the steel nozzle are slower than those originating from the glass nozzle. It stands to reason that for the steel nozzle a finer droplet size distribution is produces in comparison to the glass nozzle spray which can be decelerated more strongly. Future measurements of droplet size distributions will elucidate that phenomenon.

Summary and Conclusions

As has been shown in this paper the evaporation inside a nozzle capillary is greatly depending on the process temperature thus on the employed superheat. Evaporation is reduced for high superheating because of heat conduction phenomena. The monitoring of the evaporation in glass nozzles yields interesting hints on the behaviour for other nozzles but the evaporation will change with roughness for example. Comparing a glass and a steel nozzle it is observed that the spray disintegration is increased for the steel nozzle because of enhanced surface roughness inside the nozzle capillary that triggers a more pronounced vapour production. In addition the mass flux for the steel nozzle is smaller in comparison to the glass nozzle hinting increased evaporation which is ideal for small superheat but not for high temperatures. The effect of the modified evaporation is also noticeable regarding the velocity distributions resulting for the glass and the steel nozzle. The glass nozzle yields smaller velocities especially at the edges of the spray since the spray is not as dispersed as the spray generated by the steel nozzle yielding reduced interaction and deceleration by the surrounding gas phase.

Acknowledgements

The financial support by the German Research Foundation (DFG) within the priority program “Process Spray” (SPP 1423) is gratefully acknowledged. In addition the authors acknowledge the technical support of Markus Russ, Sebastian Knetzger, Max Braun, Sebastian Gworsek, Florian Stahl und Sabine Ziemba.

References

[1] Lefebvre A. H.; Atomization and Sprays; Hemisphere Publishing Corporation; New York 1989.

[2] J. Schröder, M.-L. Lederer, V. Gaukel, H.P. Schuchmann, Effect of atomizer geometry and rheological properties on effervescent atomization of aqueous polyvinylpyrrolidone solutions, ILASS – Europe 24rd Annual Conference on Liquid Atomization and Spray Systems, Estoril, Portugal, September 2011.

[3] E. Sher, T. Bar-Kohany, A. Rashkovan, Flash-boiling atomization, Progress in Energy and Combustion Science 34 (2008) 417 – 439.

[4] Y. Kitamura, H. Morimitsu, T. Takahashi, Critical superheat for flashing liquid jets, Ind. Eng. Chem. Fundam. 25 (1986) 206 - 211.

[5] M. Razzaghi, Droplet size estimation of two – phase flashing jets, Nuclear Engineering and Design 114 (1989) 115 - 124.

[6] A. Günther, M. Rossmeissl, K. - E. Wirth, Atomization of superheated liquids – Discharge characteristics , ILASS – Europe 23rd Annual Conference on Liquid Atomization and Spray Systems, Brno, Czech Republic, September 2010.

[7] A. Günther, K. –E. Wirth, Einfluss der Düsengeometrie auf Massenstrom und Spraycharakteristik bei überhitzer Zerstäubung, Chemie Ingenieur Technik 1-2 (2012) 149 - 153.

[8] A. Günther, K. - E. Wirth, Influence of the geometry of cylindrical nozzles on superheated atomization , ILASS – Europe 24rd Annual Conference on Liquid Atomization and Spray Systems, Estoril, Portugal, September 2011.

[9] V. A. Fedoseev, Dispersion of a stream of superheated liquid, Colloid journal 20 (1957) 463 – 466.

[10] B. S. Park, S. Y. Lee, An experimental investigation of the flash atomization mechanism, Atomization and Sprays 4 (1994) 159 - 179.

[11] Neroorkar K., Gopalakrishnan S., Grover R. O., Schmidt D. P., Simulation of flash boiling in pressure swirl injectors, Atomization and Sprays 21 (2011) 179 - 188.

Nomenclature

Roman symbols

CCD	charge coupled device	$\dot{M}$	mass flux / kgs^{-1}
$c_{p,f}$	heat capacity / $Jkg^{-1}K^{-1}$	N	number of bubbles / -
D	nozzle diameter / mm	p	pressure/ bar
Δh_v	enthalpy of vaporization / Jkg^{-1}	PIV	particle image Velocimetry
Ja	Jacob Number	q_0	number size distribution / mm^{-1}
L	length / mm	q_2	number size distribution / mm^{-1}
L/D – ratio	length – to – diameter – ratio / -	x	radius / µm
LED	light emitting diod	T	temperature / °C

Subscripts

i	*process parameter I*
f	*fluid*
v	*vapor*
sat	*saturated*
25°C	*at 25°C*
0	*starting condition*
∞	*at ambient condition*

Greek symbols

α	vapor content / -
ρ	density / kgm^{-3}
Δ	difference